Available online at www.sciencedirect.com
SCIENCE DIRECT®
Journal of Solid State Chemistry 177 (2004) 2977–2984
JOURNAL OF SOLID STATE CHEMISTRY
http://elsevier.com/locate/jssc

Magnetic and electronic structure of $TlCo_2S_2$

Sabina Ronneteg,[a,*] Marck-Willem Lumey,[b] Richard Dronskowski,[b] Ulrik Gelius,[c] Rolf Berger,[a] Solveig Felton,[d] and Per Nordblad[d]

[a] *Department of Materials Chemistry, Ångström Laboratory, Uppsala University, Box 538, SE-751 21 Uppsala, Sweden*
[b] *Institut für Anorganische Chemie, Rheinisch-Westfälische Technische Hochschule, Prof.–Pirlet-Str. 1, D–52056, Aachen, Germany*
[c] *Department of Physics, Ångström Laboratory, Uppsala University, Box 530, SE-751 21 Uppsala, Sweden*
[d] *Department of Materials Science, Ångström Laboratory, Uppsala University, Box 534, SE-751 21 Uppsala, Sweden*

Received 17 December 2003; received in revised form 29 April 2004; accepted 30 April 2004

Available online 24 June 2004

Abstract

An extensive investigation of the ferromagnetic compound $TlCo_2S_2$ has resulted in new information on the electronic and magnetic structure. Electronic structure calculations showed that magnetic ordering is energetically favorable with a clear driving force for ferromagnetic coupling within the cobalt layers. $TlCo_2S_2$ is metallic and the conductivity is due to holes in the valence band. XPS single crystal measurements did not show evidence of mixed oxidation states of cobalt. Neutron powder diffraction resulted in a ferromagnetic structure with the magnetic moment in the *ab*-plane. The derived magnetic moment of the cobalt atom is $0.65(2)\,\mu_B$ at 10 K and is in very good agreement with the value, $\mu_{sat} = 0.65(1)\,\mu_B$ at 10 K, inferred from the magnetic hysteresis curve.

Keywords: Ferromagnetism; Magnetism; $ThCr_2Si_2$ type; $TlCo_2S_2$; COHP; Layered magnetic structure; XPS; SQUID; Neutron diffraction

1. Introduction

The $ThCr_2Si_2$ type family ($I4/mmm$) is interesting due to the large variations in properties that different representatives of this layered structure exhibit [1,2]. In the structure (Fig. 1), with formula AT_2X_2, the X atoms are *p*-elements, often silicon or germanium, which form a cubic coordination around the A atoms. In 1978, Klepp and Boller reported the first chalcogenides of the $ThCr_2Si_2$ type structure [3]. The transition metal T atoms form sheets with a square planar coordination at a distance quite similar to that of the pure T metal. Each T atom is surrounded by a tetrahedron of X atoms. In magnetic studies of the $ThCr_2Si_2$ family, it is common that the rare earth element in the A position is magnetic [4] and sometimes also the T atom. It is quite rare that only the T atom possesses a magnetic moment. If the A and X are diamagnetic large atoms and T is a paramagnetic 3*d* metal, the compound gets an enhanced two-dimensional structure with a large separation between the T layers. Such a structure contains two radically different magnetic interaction distances.

Compounds that fulfil these criteria are $TlCo_2X_2$ (X = S, Se). The sulphide $TlCo_2S_2$, which is in the focus of this paper, is a ferromagnetic layered structure with $T_C = 150-154$ K [5–7] and with the cobalt magnetic moment oriented along the tetragonal *a*-axis [6]. In contrast, the selenide $TlCo_2Se_2$ is antiferromagnetic [8,9]. However, both structures have a ferromagnetic coupling within the metal sheets due to direct interactions. The closest Co–Co distances are ~2.6 Å as four near neighbors. The difference in the net magnetic behavior is traced to the large distance (~6.5 Å) between the layers, with a coupling probably due to interactions mediated by the conduction electrons. In a more thorough investigation of $TlCo_2Se_2$ this interaction was found to be an incommensurate non-collinear antiferromagnetic coupling [10] compared to a ferromagnetic one for the sulphide. These new findings inspired us to also search for a more detailed picture of the magnetic and electronic structure of the

*Corresponding author. Fax: +4618513548.
E-mail address: sabro@mkem.uu.se (S. Ronneteg).

0022-4596/$ - see front matter © 2004 Elsevier Inc. All rights reserved.
doi:10.1016/j.jssc.2004.04.057

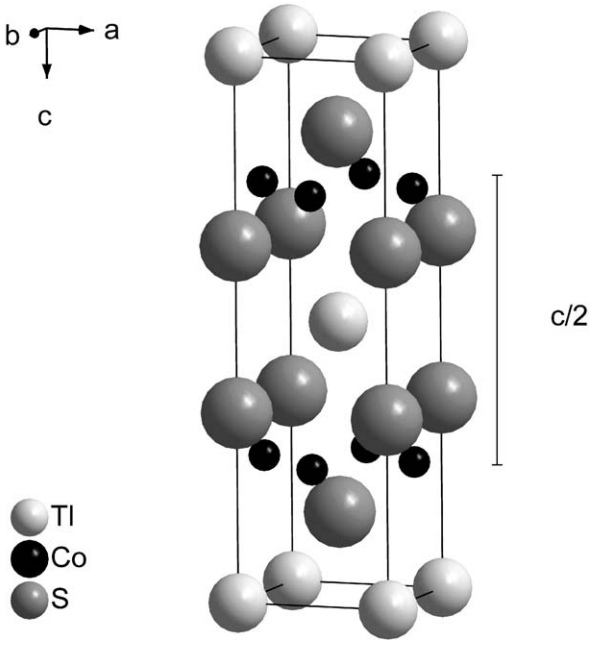

Fig. 1. The unit cell of the tetragonal structure of $TlCo_2S_2$.

ferromagnetic $TlCo_2S_2$. The system was investigated by magnetometry, XPS and neutron powder diffraction, with support from electronic structure calculations. Neutron diffraction was used to confirm the suggested magnetic structure and determine the magnetic moment. X-ray photoelectron spectroscopy (XPS) has earlier been used for investigating $TlCu_2X_2$ (X = S, Se) [11]. These compounds are metallic due to holes in the valence-band, and the formal oxidation state of copper is Cu(I), d^{10}. Correspondingly, XPS was used to gain bonding information in $TlCo_2S_2$. The experimental study was combined with theoretical calculations to get a better interpretation of the valence-band data and further insight into the driving force for the magnetic interactions.

Our study of $TlCo_2S_2$ is part of a more extensive investigation of the antiferro- to ferromagnetic transition in the $TlCo_2Se_{2-x}S_x$ system.

2. Experimental

2.1. Synthesis

$TlCo_2S_2$ powder was synthesized by mixing stoichiometric amounts of the elements. The materials were brought to melting in an evacuated silica-tube and homogenized twice, being heat-treated at 873 K. Single crystal material was prepared by first bringing $TlCo_2S_2$ powder to melting in an evacuated silica-tube. The melt was then slowly cooled to room temperature. The resulting solidified ingot showed strong preferred orientation and split easily through cleavage by a scalpel. The crystal used for XPS had a flat elliptical shape, with a diameter of approximately 5 mm. The flat surfaces were of the {001} orientation.

2.2. Diffraction

The powder sample was investigated by X-ray diffraction in a Guinier-Hägg camera, using Cu$K\alpha_1$ radiation and germanium ($a = 5.6570805$ Å at 295.6 K [12]) as internal calibration standard. The quality of the $TlCo_2S_2$ single crystal was ascertained by X-ray diffractometry (Siemens D5000, parabolic X-ray mirror on the primary side and a parallel plate collimator in front of the detector, Cu$K\alpha$ radiation) by recording a φ-scan and a rocking-curve. Neutron diffraction measurements were performed on the Neutron Powder Diffractometer (NPD, wavelength 1.47 Å) in Studsvik, Sweden. Five sets of data were collected, at 295, 160, 140, 80 and 10 K. The profile fitting refinements were made using the Fullprof program [13].

2.3. Magnetic measurements

The magnetic measurements were performed on a SQUID magnetometer (Quantum Design, MPMS XL5). The magnetization was recorded as a function of temperature between 10 and 300 K with an applied field of 200 Oe, for both powder and single crystals. Magnetization vs. temperature scans was also performed in a limited temperature range close to T_C in a weak magnetic field, $H = 10$ Oe, to determine the Curie temperature of the system more accurately. For the evaluation of the saturated moment on powder, full hysteresis curves were recorded up to 10 kOe at 10 and 80 K.

2.4. XPS

The XPS measurements were performed with a Scienta ESCA-300 spectrometer using monochromated Al$K\alpha$ X-ray excitation [14]. The $TlCo_2S_2$ single crystal was mechanically mounted on a standard sample holder with aluminium foil underneath, and a Scotch tape was gently pressed onto the available upper crystal surface. The sample was then introduced into the load-lock chamber and pumped down to the low 10^{-7} mbar range in about 5 min, followed by a transfer to the adjacent preparation chamber. This chamber, pumped by a Ti-sublimation pump in combination with an oil-free Seiko Seiki STP-400 turbomolecular pump (magnetic bearings), has a base pressure of about 5×10^{-11} mbar.

After a few minutes, the pressure in the preparation chamber reached the low 10^{-10} mbar range. The tape was then pulled off the crystal by a wobble stick equipped with a gripping pincer, so that an almost

perfect UHV-cleaved surface was obtained. Only a few percent of the crystal surface was not perfectly stripped.

The UHV-peeled crystal was then inserted into the analysis chamber and placed onto a universal manipulator. The electron take-off angle was chosen to be 90° in order to make the XPS analysis as bulk sensitive as possible. The lateral and polar orientations of the crystal were adjusted to minimize the O 1*s* and C 1*s* line intensities from less perfect edges of the crystal.

3. Electronic calculations

The electronic structure calculations were performed using the Linear Muffin-Tin Orbital (LMTO) theory [15–17] in its tight-binding representation. The program used was TB-LMTO 4.7 [18]. Electronic energies were calculated via density-functional theory (DFT), and the exchange-correlation parts were treated in the local density approximation (LDA) as parameterized by von Barth and Hedin [19]. For expressing the bonding character, the crystal orbital Hamilton population COHP [20] was used. This method is in many ways analogous to crystal orbital overlap population COOP [21]. The difference is that COOP is a Mulliken overlap population weighted density-of-states, while COHP instead is a Hamiltonian population weighted density-of-state. By doing so, we partition the band structure energy into bonding, non-bonding and antibonding contributions. The bonding state for the COHP has a negative sign (compared to COOP's positive sign) due to the gain in energy. For easier comparison between the two representations, –COHP is plotted.

For itinerant systems susceptible to large exchange splittings, it has been pointed out [22] that a high antibonding character of the levels close to the Fermi edge in the non-spin-polarized COHP is a fingerprint for spin polarization; for the 3*d* metals this results in spontaneous ferromagnetism. By allowing for two spin sub-lattices in the system, the electronic symmetry can be reduced, increasing variational freedom and thus gaining energy. At the same time, the metal–metal antibonding states at the Fermi level become annihilated. Electrons with the same spin repel each other more than electrons with different spin. The outcome is a difference in the amount of spin-up and spin-down electrons, which results in magnetic ordering and less antibonding density at the Fermi level. This perturbation is very small compared to the Coulomb forces in the system but is still very significant for the magnetism of transition metals and their compounds. The strength of the chemical bonds in the compound can be studied by integrating the COHP (ICOHP).

Calculations were performed with and without spin polarization. In the spin-polarized case, two different calculations were made. The first was an ordinary spin calculation with all cobalt atoms equal, resulting in a ferromagnetic interaction. In the second one, the symmetry of the unit cell was reduced (to *P*4*mm*, same size of the unit cell as $I4/mmm$) to allow for two cobalt positions, one for each layer. This reduction makes it possible to form an antiferromagnetic coupling between the layers. In the following, these three calculations are referred to as non-magnetic, ferromagnetic and antiferromagnetic. Some calculations were also made where different unit cell axes were used, to study how stable or unstable the system was to change. The irreducible Brillouin zone was sampled with a $48 \times 48 \times 16$ *k*-point mesh for the total energy calculations, which resulted in 5861 irreducible *k*-points in $I4/mmm$ and 5200 in *P*4*mm*.

4. Results and discussion

4.1. Electronic structure

The φ-scan of the flat crystal showed that it was a single crystal with fourfold symmetry. However, the rocking-curve indicated a mosaic structure shown by a peak split. The quality of the $TlCo_2S_2$ was still considered good enough for the XPS measurement, being single phase.

Survey spectra ($0 \rightarrow 1000$ eV, 500 eV pass energy) and detail spectra, Tl 4*f*, Co 2*p*, S 2*p* and valence band ($22 \rightarrow -3$ eV, 300 eV pass energy) were recorded for three different UHV cleaved surfaces, showing different amounts of O 1*s* and C 1*s* contaminations (Fig. 2a). The spectra from the best cleavage gave almost identical Co 2*p*, S 2*p*, Tl 4*f* and valence band spectra as the second best cleavage, that had only slightly higher O 1*s* and C 1*s* signals. The carbon and oxygen contaminations for the best cleavage were estimated as 6 and 1.5 atomic percent, respectively. Fig. 2 shows the total spectrum and those of Co 2*p*, S 2*p*, Tl 4*f* and the valence band. The electron binding energies of the different core electron levels are listed in Table 1. The shape and position of the C 1*s* peak indicates that this mainly originates from the glue from the Scotch tape, from the small areas that did not peel off. Also, the oxygen signal could entirely be attributed to originating from this glue. Since the valence electrons in the investigated valence band region ($\leqslant 22$ eV) of carbon and oxygen have lower photoionization cross sections than those of the valence electrons of the other elements, their intensity contribution to the studied valence band region is in practice totally negligible. In view of these measures, the VB and core spectra seem reliable enough for a valid interpretation of the binding situation. However, this interpretation is by no means easy in all parts.

The valence band is depicted in Fig. 2e and f. The Fermi edge (zero binding energy) obviously cuts the VB near the top, with states mainly composed of

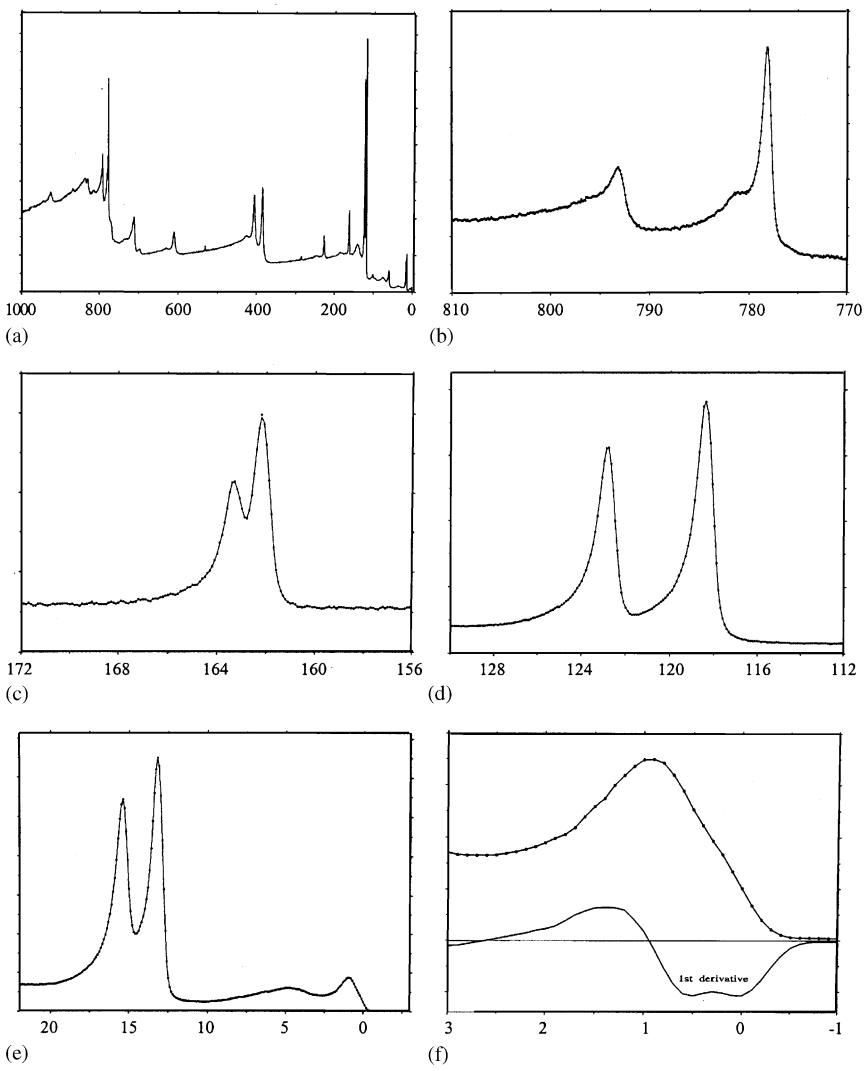

Fig. 2. The XPS spectra of $TlCo_2S_2$, the total spectrum (a), Co 2*p* (b), S 2*p* (c), Tl 4*f* (d), and the valence band (e) with Tl 5*d* peaks. In (f) a blow-up of part of the spectrum in (e) is shown, together with the derivative for a more detailed profile analysis. The intensities are given only on a relative scale, while the horizontal axes give the binding energy in eV with the Fermi edge at zero.

Table 1
Experimental core electron binding energies for the elements in $TlCo_2S_2$

Core electron level	Electron binding energy (eV)
Co $2p_{1/2}$	793.17
Co $2p_{3/2}$	778.15
S $2p_{3/2}$	162.17
Tl $4f_{5/2}$	122.85
Tl $4f_{7/2}$	118.40
Tl $5d_{3/2}$	15.42
Tl $5d_{5/2}$	13.16

(Reference level: Ag $3d_{5/2}$ at 368.27 eV).

narrow-band features. There is a small but pronounced shoulder just below zero, accentuated in Fig. 2f. Metallic conductivity is expected which, accordingly, has been confirmed from measurement [7]. Within the range of 5 eV from the Fermi level, there are two distinct band features that should contain Co 3*d* states to a large extent. Considering the expected crystal field effects of the tetrahedral cobalt coordination towards sulfur as well as the quasi-two-dimensional character of the cobalt sheets, the humps at 1 and 5 eV, respectively, reflect a situation of a marked partitioning of the 3*d* manifold into mainly two sets. The 5 eV hump should contain a larger extent of sulfur based states (Co–S bonding, compare with Fig. 4d–f).

The holes at the VB top lie close enough to affect the Co 3*d* states, with holes also in the *d*-band. As a result, a situation of mixed Co valency is expected which might also influence the XPS signal of the Co 2*p* core states, yielding the possibility of satellites. However, the corresponding spectrum (Fig. 2b) is difficult to interpret. An intensity ratio of 2:1 is expected between the $2p_{3/2}$ and $2p_{1/2}$ states. These features are obscured by two

effects, a tailing tendency towards higher energy and overlapping Auger states, the latter more pronounced for the $2p_{3/2}$ peak. The tailing asymmetry is found also for the Tl 4*f*, Tl 5*d* and S 2*p* spectra, all indicative of the metallic character by itinerant electron states.

For the LMTO calculations the crystallographic data were taken from the neutron diffraction refinement for 10 K (see Table 3). The result is summarized in Table 2. The total energy of the two magnetic calculations is lower than the non-magnetic one. However, the difference between the ferromagnetic and the antiferromagnetic calculation is hardly significant.

In Fig. 3, the density-of-states (DOS) in the valence band region is drawn for the three calculations. There is a peak in the density-of-states in the non-magnetic case at the Fermi level. By allowing for spin polarization, the density decreases at the Fermi energy due to a split between the spin-up and the spin-down electron curves. This is energetically favorable. The Co 3*d* and the S 3*p* states are strongly mixed which indicates the expected covalent bond. The density-of-states (DOS) curve is roughly comparable to the XPS result in Fig. 2e–f. However, the XPS was done at room temperature where excited states are involved, whereas the calculations are performed at 0 K and only involves the ground states. Moreover, the XPS data are weighted by electron hole excitations and different element sensitivity.

Table 2
Results from the LMTO-ASA calculations

	Nonmagnetic	Ferromagnetic	Antiferromagnetic
E_{tot} (kJ/mol)[a]	0	−3.7	−3.3
ICOHP (kJ/mol)[b]	0	−3.0	−2.7
μ_{sat} Tl (μ_B/atom)	—	0.06	0.00
μ_{sat} Co (μ_B/atom)	—	0.81	0.79
μ_{sat} S (μ_B/atom)	—	0.06	0.06

The values are normalized to the nonmagnetic calculation.
[a] Per formula unit.
[b] Four identical bonds in one sheet in the unit cell.

For the COHP calculation, the nearest Co–Co and Co–S bonds are illustrated for both non-magnetic and magnetic calculations in Fig. 4. In the non-magnetic COHP (Fig. 4a) the largest decrease in energy was shown in the nearest neighbor Co–Co bond (2.64 Å). Here, the high density of antibonding states at the Fermi level is very clear and is an indication of electronic instability where spin polarization respectively magnetism can lower the energy. Fig. 4b and c shows how the density of filled states decreases when spin polarization is allowed in the calculations while the spin-up and the spin-down curves separate. The stabilization is also shown in the ICOHP values (Table 2). If we compare the antiferromagnetic and the ferromagnetic total energies, as well as the ICOHP, there are no significant differences. The reason is that the coupling between the sheets is out of reach (being more than 6 Å apart) for the electronic structure theory and the approximations in LMTO.

4.2. Magnetic structure

Our magnetic measurements show that $TlCo_2S_2$ is a ferromagnetic compound, and the weak field measurement yields $T_C = 146$ K, which is a little lower than earlier published results of $T_C = 150-154$ K [5–7]. The measurements on two different single crystals showed that the magnetic moment is perpendicular to the *c*-axis,

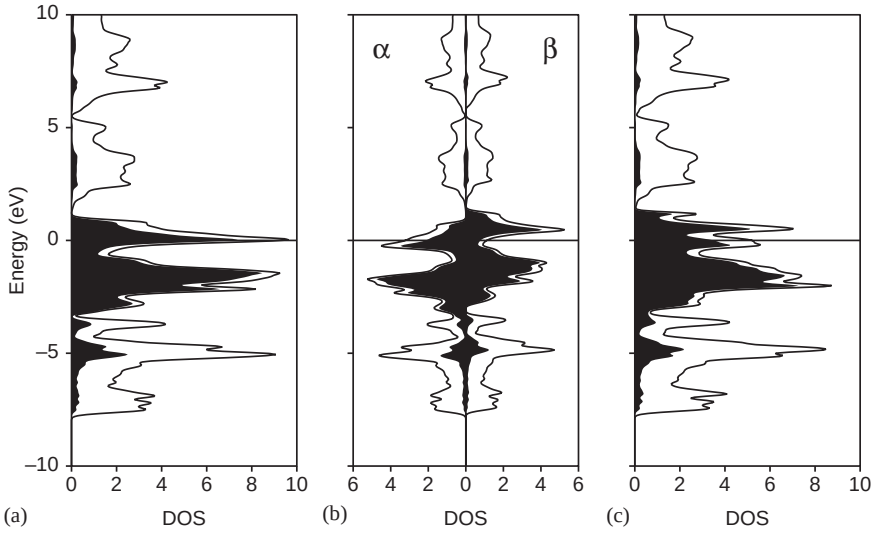

Fig. 3. Density-of-states (DOS) with local Co 3*d* projections in black for the non-magnetic (a), ferromagnetic (b) and antiferromagnetic (c) structure. In 3b the alpha/beta spins are plotted separately. They correspond to the majority resp. minority spin. All curves have been shifted in energy so that the Fermi level lies at 0 eV.

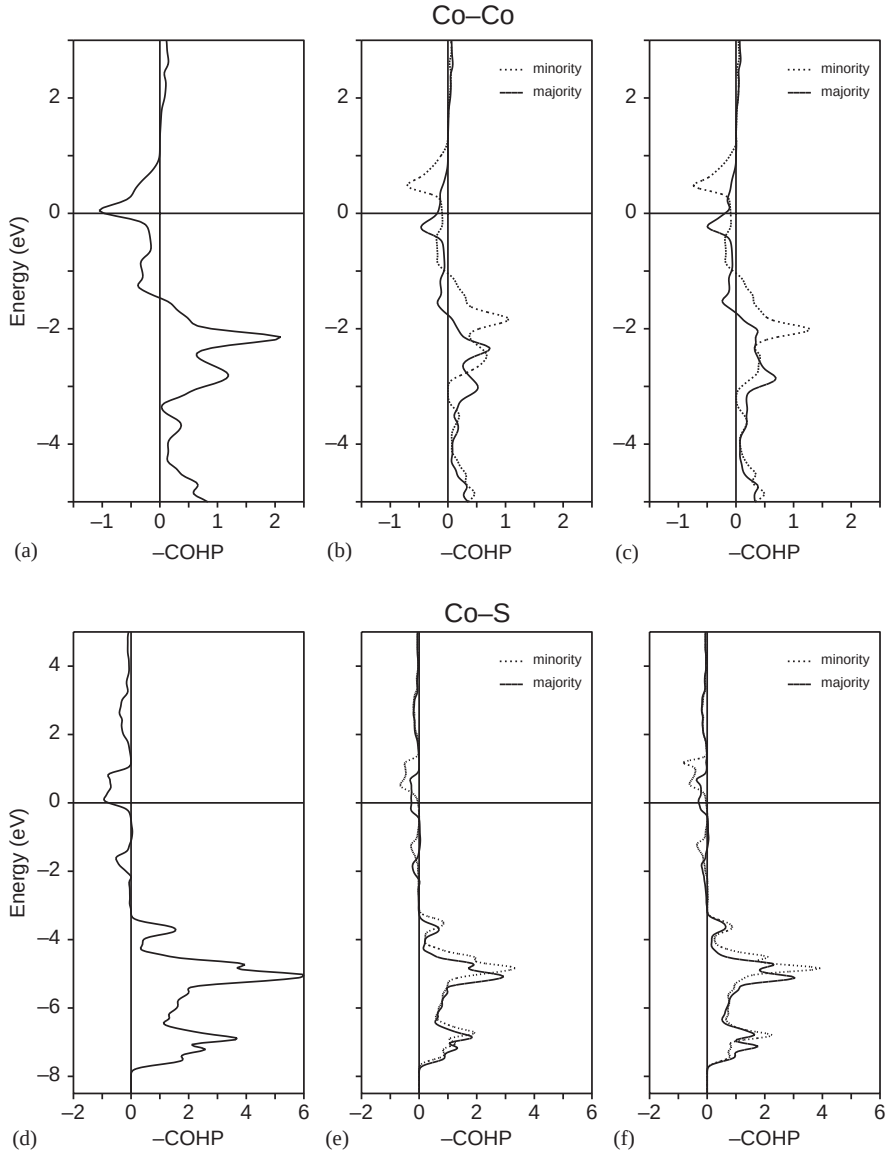

Fig. 4. Crystal orbital Hamilton populations (COHP) of the Co–Co bond at 2.64 Å (a–c) and the Co–S bond at 2.25 Å (d-f) for the non-magnetic (a,d), ferromagnetic (b,e) and antiferromagnetic (c,f) structure. Note that the –COHP is drawn. This means that the bonding state has a positive sign, while the antibonding is negative.

but the quality of the crystals was not good enough for determining the orientation in the *ab*-plane. In powder neutron diffraction, extra intensity of the (002) peak due to ferromagnetism started in the cooling mode to appear at 140 K (nothing at 160 K). The profile refinements showed a ferromagnetic structure with the cobalt moment in the *ab*-plane. Two neutron diffractograms are shown in Fig. 5. The increase in intensity on cooling is the only notable change in the diffractograms indicating this transition, except for a minor contamination of CoO found at $2\theta \approx 17°$. The results from the refinements are shown in Table 3.

The saturated magnetic moment from the magnetic hysteresis curves is 0.66(1) μ_B at 10 K (Fig. 6) and 0.59(1) μ_B per cobalt atom at 80 K. This agrees very well with the neutron diffraction refinements (Table 3). This value can be compared to the result by Huan et al. [5,7], namely 1.09 μ_B per formula unit (0.545 μ_B per cobalt atom). $TlCo_2S_2$ is a very soft magnetic material with no visible hysteresis. The inverse susceptibility in the temperature range 180–300 K is adequately described by a Curie–Weiss law which yields an effective magnetic moment of 2.9 μ_B per formula unit and a Curie–Weiss temperature of 163 K. This value of the effective magnetic moment agrees with earlier findings of 2.62–3.07 μ_B [5–7].

The magnetic moment from the LMTO calculations (Table 2) on $TlCo_2S_2$ is located at the cobalt atoms as

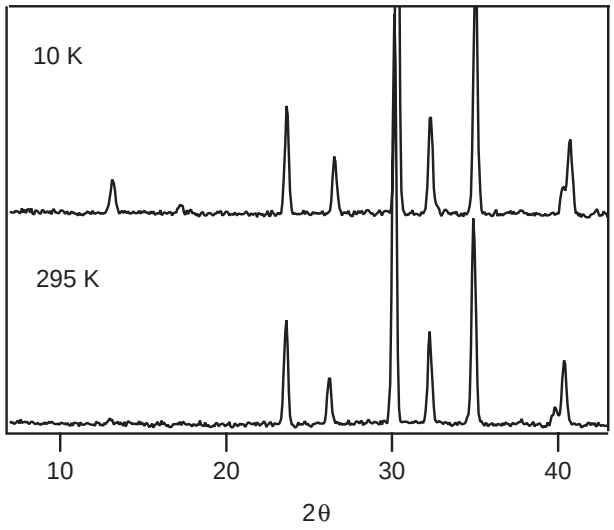

Fig. 5. Results from powder neutron diffraction at 295 and 10 K.

Table 3
Results from the Rietveld refinements of the powder neutron diffraction data in the range $5<2\theta<90$

	295 K	160 K	140 K	80 K	10 K
a (Å)	3.7419(2)	3.7367(1)	3.7363(1)	3.7369(1)	3.7367(1)
c (Å)	12.957(1)	12.891 (1)	12.875 (1)	12.841(1)	12.810(1)
z_S	0.3468(3)	0.3472(3)	0.3469(3)	0.3473(3)	0.3472(3)
R_{cryst} (%)	4.63	4.25	3.73	3.69	3.85
μ_{sat} Co (μ_B)[a]	—	—	0.36(3)	0.57(2)	0.65(2)
R_{mag} (%)	—	—	9.06	11.74	9.12

[a] Magnetic moment is perpendicular to the c-axis.

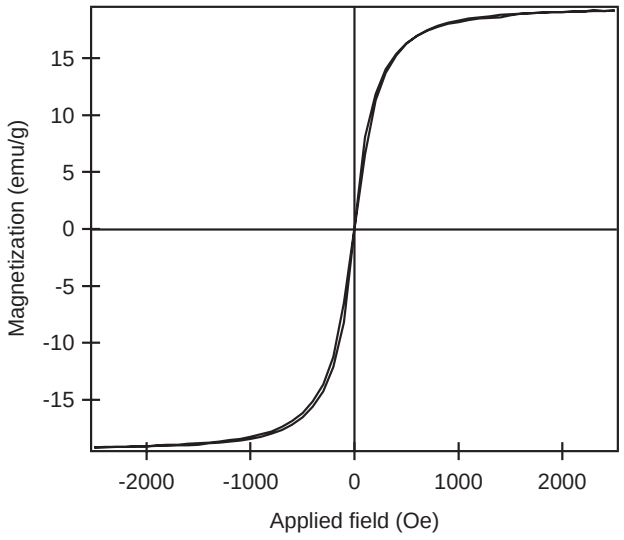

Fig. 6. Magnetic saturation measurement at 10 K (the measurement was done up to 10 kOe but only a part of it is illustrated in the figure).

expected. The magnetic moment calculated is a little larger than found experimentally, but the values are still of the same magnitude.

5. Conclusions

$TlCo_2S_2$ is a ferromagnetic layered compound with the magnetic moment located around the cobalt atoms and perpendicular to the c-axis. Neutron powder diffraction confirmed the expected tetragonal magnetic structure, but no information could be gained concerning the direction of the magnetic moment within the ab-plane. Both neutron diffraction and magnetic measurements gave a magnetic moment at 10 K of 0.65 μ_B. $TlCo_2S_2$ is metallic, the conductivity being explained from XPS and calculations as due to valence band holes. This would indicate low cobalt oxidation states. We cannot see any distinct proof of mixed valence states of the cobalt atoms from the XPS data. The theoretical calculations show a clear driving force for a ferromagnetic coupling in the cobalt layers.

Calculations were also performed when the unit cell parameters in the structure were changed, to see how stable the magnetic interactions were. The ferromagnetic stability in the sheets does not seem to be very dependent on the Co–Co distance in the layer and unfortunately, the large c-axis brings the interlayer interactions out of reach. For comparison, we also performed calculations on antiferromagnetic $TlCo_2Se_2$, and we could clearly confirm the ferromagnetic interaction within the cobalt layer, but for the same reason as above we were unable to handle the long-range interactions that create the antiferromagnetism.

Now knowing in detail how the end compounds of the system $TlCo_2Se_{2-x}S_x$ behave, we intend to proceed with their solid solutions. The system has been investigated earlier [5] but we will study more in detail how the properties and magnetic structure change when the interlayer distance is tuned.

Acknowledgments

Financial support from the Swedish Foundation for Strategic Research (SSF), the Foundation in Memory of Bengt Lundqvist, the Gertrud Thelin Foundation and Ångpanneföreningen's Foundation for Research and Development is thankfully acknowledged. We are grateful to Mr. Håkan Rundlöf at the Studsvik nuclear reactor facility for recording the neutron diffraction data. S.R. expresses her gratitude for the invaluable stay in Aachen at the Institut für Anorganische Chemie at RWTH.

References

[1] Z. Ban, M. Sikirica, Acta Crystallogr. 18 (1965) 594–599.
[2] P. Paufler, G. Just, J. Alloys Compd. 232 (1996) 1–25.
[3] K. Klepp, H. Boller, Monatsh. Chem. 109 (1978) 1049–1057.

[4] A. Szytula, J. Leciejewicz, in: K.A. Gschneidner, Jr., L. Eyring (Eds.), Handbook on the Physics and Chemistry of Rare Earths, Vol. 12, p. 133, Elsevier, Amsterdam, 1989.
[5] M. Greaney, G. Huan, K.V. Ramanujachary, Z. Teweldemedhin, M. Greenblatt, Solid State Commun. 79 (1991) 803–810.
[6] G. Huan, M. Greenblatt, K.V. Ramanujachary, Solid State Commun. 71 (1989) 221–228.
[7] G. Huan, M. Greenblatt, M. Croft, Eur. J. Solid State Inorg. Chem. 26 (1989) 193–220.
[8] G. Huan, M. Greenblatt, J. Less-Common Met. 156 (1989) 247–257.
[9] A.R. Newmark, G. Huan, M. Greenblatt, M. Croft, Solid State Commun. 71 (1989) 1025–1032.
[10] R. Berger, M. Fritzsche, A. Broddefalk, P. Nordblad, B. Malaman, J. Alloys Comp. 343 (2002) 186–191.
[11] L. Karlsson, M.P. Keane, R. Berger, J. Less-Common Met. 166 (1990) 353–365.
[12] J.F.C. Baker, M. Hart, Acta Crystallogr. A 31 (1975) 364–367.
[13] L.L.B.C.-C. Full, Prof program by J. Rodriguez-Carvajal, Laboratoire Leon Brillouin (CEA-CNRS), Saclay, France.
[14] U. Gelius, B. Wannberg, P. Baltzer, H. Fellner-Feldegg, G. Carlsson, C.G. Johansson, J. Larsson, P. Muenger, G. Vegerfors, J. Electron. Spectrosc. Relat. Phenom. 52 (1990) 747–785.
[15] O.K. Andersen, Phys. Rev. B 12 (1975) 3060–3083.
[16] H. Skriver, The LMTO Method, Springer, Berlin, 1984.
[17] O.K. Andersen, O. Jepsen, Phys. Rev. Lett. 53 (1984) 2571–2574.
[18] G. Krier, O. Jepsen, A. Burkhardt, O.K. Andersen, The TB-LMTO-ASA program, Version 4.7, Stuttgart, Germany.
[19] U. von Barth, L. Hedin, J. Phys. C 5 (1972) 1629–1642.
[20] R. Dronskowski, P.E. Blöchl, J. Phys. Chem. 97 (1993) 8617–8624.
[21] T. Hughbanks, R. Hoffmann, J. Am. Chem. Soc. 105 (1983) 3528–3537.
[22] G.A. Landrum, R. Dronskowski, Angew. Chem. Int. Ed. 39 (2000) 1560–1585.